Multi-body dynamic modelling and flight control for an asymmetric variable sweep morphing UAV

L. Tong
wwtonglei@gmail.com
H. Ji
jihb@ustc.edu.cn
Department of Automation
University of Science and Technology of China
Hefei, China

ABSTRACT

In this paper, the multi-body dynamic model of an asymmetric variable sweep wing morphing UAV is built based on Kane's method. This model describes the UAV's transient behaviour during morphing process and the dynamic characteristic of the variable sweep wings. An integrated design of trajectory tracking control via constrained backstepping method is presented then. The idea of aircraft roll control through asymmetric wing sweep angle changes rather than traditional aileron is explored and used in the flight control design. The control of variable sweep wings is designed as well based on the presented dynamic model. Command filters are used in the backstepping design procedure to accommodate magnitude, rate and bandwidth constraints on virtual states and actuator signals. Stability of the closed-loop system can be proved in the sense of Lyapunov. Simulation of tracking a desired trajectory which contains two manoeuvres demonstrates the feasibility of the proposed protocol and the morphing wing roll controller.

Paper No. 4020. Manuscript received, 18 June 2013, accepted 4 July2014.

https://doi.org/10.1017/S000192400000943X Published online by Cambridge University Press

NOMENCLATURE

(p, q, r)	angular velocity
(u, v, w)	body co-ordinate airspeed
(x, y, z)	co-ordinate of O_f in $\{I\}$
α	attack angle
β	sideslip angle
η_l ,η_r	time derivatives of H_l and H_r
Γ	variable sweep UAV system
Q	matrix relates $[p\ q\ r]^T$ to $[\dot{\phi}\ \dot{\theta}\ \dot{\varphi}]^T$
ϕ, θ, Ψ	attitude angles
$\vec{\omega}_1^F, \ldots, \vec{\omega}_8^F$	partial angular velocities of F_L
V	airspeed
$\vec{v}_1^F, \ldots, \vec{v}_8^F$,	partial velocities of O_f
$\{I\}$	earth co-ordinate system
$\{B\}$	body co-ordinate system
C_D	drag coefficient
C_L	lift coefficient
$F_j (j = 1, \ldots, 8)$	generalised active forces of Γ
$F_{fj} (j = 1, \ldots, 8)$	generalised active forces of FL
$F_{lj} (j = 1, \ldots, 8)$	generalised active forces of W_l
$F_{lj}^* (j = 1, \ldots, 8)$	generalised inertia forces of W_l
$F_{rj} (j = 1, \ldots, 8)$	generalised active forces of W_r
$F_{rj}^* (j = 1, \ldots, 8)$	generalised inertia forces of W_r
FL	fuselage
k_L	drag-to-lift ratio
M_f	mass of FL
O	CG of Γ
O_1,O_2	connecting points of wings and fuselage
O_f	CG of FL
O_l, O_r	CG of W_l and W_r
P, Q, F, G	matrix functions
t	time
UAV	unmanned air vehicle
W_l ,W_r	two wings
δ_η	differential wing sweep angle morphing
δ_e, δ_r	control-surface deflections
γ, χ, μ	flight path angles
$\vec{I}f$	central inertia dyadic of FL
H_l, H_r	wing sweep angles
$\vec{\alpha}_f$	angular acceleration of FL
$\vec{\Omega}_f$	angular velocity of FL
$\vec{a}_{Of}$	acceleration of O_f
$\vec{G}_f$	gravity of FL
$\vec{R}_f^*$	inertia force of FL
$\vec{R}_l^*$, $\vec{R}_r^*$	inertia forces of W_l and W_r
$\vec{T}_f^*$	inertia torque of FL

https://doi.org/10.1017/S000192400000943X Published online by Cambridge University Press

$\vec{T}_l^*, \vec{T}_r^*$	inertia torques of W_l and W_r
$\vec{V}_{Of}$	velocity of O_f in $\{I\}$
$F_j^*(j = 1, ..., 8)$	generalised inertia forces of Γ
$F_{fj}^*(j = 1, ..., 8)$	generalised inertia forces of FL
$J_F, J_A, J_T, E_G, K_V, K_\Omega, K_\eta, N$	coefficient matrices
$\vec{\omega}_1^L, ..., \vec{\omega}_8^L$	partial angular velocities of W_l
$\vec{\omega}_1^R, ..., \vec{\omega}_8^R$	partial angular velocities of W_r
$\vec{D}_f$	aircraft zero lift drag
$\vec{d}_F, \vec{d}_Y, \vec{d}_L, \vec{d}_D$	position vectors
$\vec{F}_B$	thrust force of aircraft engines
$\vec{L}_t$	lift force of the horizontal tail
$\vec{M}_\eta$	roll moment generated by differential wing sweep angle
$\vec{R}_f$	equivalent force of FL
$\vec{R}_{wl}, \vec{R}_{wr}$	equivalent forces of W_l and W_r
$\vec{T}_f$	equivalent torque of FL
$\vec{T}_l, \vec{T}_r$	control torques of variable sweep wings
$\vec{T}_{wl}, \vec{T}_{wr}$	equivalent torques of W_l and W_r
$\vec{v}_{L1}, ..., \vec{v}_{L8}$	partial velocities of O_l
$\vec{v}_{R1}, ..., \vec{v}_{R8}$	partial velocities of O_r
Y_t	The aerodynamic force of the rudder
S_M, S_R	Saturation functions
$B_{\vec{z}}$	The unit vector along $\{B\}$'s z axis
${}_I^B R$	The rotation matrix from $\{I\}$ to $\{B\}$

1.0 INTRODUCTION

With the development of control science, material science and microelectronics, unmanned air vehicles (UAV) have been widely used in both military and civil applications[1,2]. Natural advantages, including no human physiological limits needed to be considered, simplicity of design and relatively low price have made UAVs an excellent experimental platform for new technologies.

One of the rising topics of interest for researchers is the combination of UAV and aircraft morphing. As has been proved by many studies and aircraft like the F-14 Tomcat, morphing technologies, such as variable sweep, variable span and other kinds of large-scale morphing, can highly improve an aircraft's performance in different flight scenarios[3-7]. The weak sides of morphing that prevent it from been widely used, on the other hand, include the complexity of mechanism, difficulties in modelling and control design and lack of safety guarantee. However, when applied to a UAV, many defects of morphing can be neglected. Nowadays, much researchabout morphing is carried out on a UAV platform. Lockheed Martin flight-tested a UAV with folding-wing morphing, while DARPA used a UAV as a technology demonstrator of morphing in flight[8]. M. Abdulrahim and R. Lind *et al* built a UAV with a biologically-inspired morphing mechanism and their studies showed significant benefit from morphing for small vehicles[8-11]. C.H. Hong and M. Cheplak *et al* designed a multi-body UAV capable of significant geometric morphing to incorporate wing area and sweep angle change[12].

While most of the studies consider that the shape change was done in an open-loop manner, some researchers have begun to use structural changes as additional (dynamic) aerodynamic forcing inputs for aircraft control[13]. A.C. Hurst *et al* presented an adaptive aircraft with morphing control input that allows it to land through a perching manoeuvre [14]. P. Bourdin *et al* presented a novel

https://doi.org/10.1017/S000192400000943X Published online by Cambridge University Press

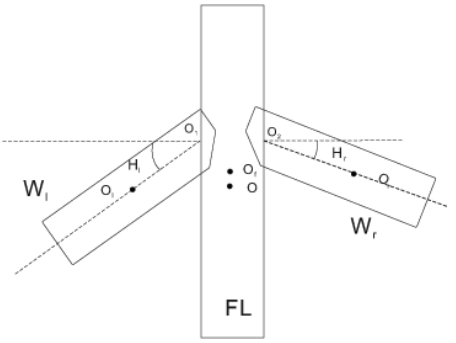


Figure 1. Asymmetric variable sweep UAV model Γ.

method for the control of aircraft by using articulated split wing-tips[15]. J.J. Henry explored the idea of aircraft roll control through asymmetric variable span morphing[16].

The effects of the asymmetric variable sweep mechanism were studied in Ref. 17 and the idea of using it as the roll controller was presented in Ref. 18. The basic idea is that the asymmetric wing sweep morphing can lead to a lift difference between two wings, which yields a roll moment without the help of ailerons. In this paper, the asymmetric wing sweep morphing is used as the roll controller and incorporated with trajectory tracking control of the UAV.

For a morphing UAV capable of large scale shape change, it is not suitable to treat it as a single rigid body because of complex interactions between inertial forces and aerodynamic forces. Here the asymmetric variable sweep UAV is considered as a three-body system with its two wings allowed to sweep independently.

There are many ways to model a multi-body system, such as the Newton-Euler method or Lagrange's Equations. In this paper, a classic approach proposed by Thomas R. Kane during the 1970s and 1980s is used to model the UAV system[19]. There have been many discussions among Kane's method, Lagrange's equations and Gibbs-Appell's equations. Essentially, they give the same result for a multi-body system but Kane's method is more suitable for computer programming and analysis[20-22]. The presented model describes the transient behavior of the UAV during the wing sweep morphing process. Dynamic equations of the asymmetric sweep wings are also contained, which makes it possible for the morphing control design. The guidance equations used in this paper can be found in Ref. 23.

Trajectory tracking is often required for a UAV in various kinds of mission scenarios. To achieve better stability guarantee and improve performance, here the guidance and control laws are designed in an integrated way[24]. As a Lyapunov function-based design method, backstepping method is suitable for handling high-order nonlinear systems with lower-triangular form. However, it can not handle physical limitations of control surfaces, especially the wing morphing limitations when applied to the asymmetric variable sweep UAV control design. The constrained backstepping approach presented in Refs 25-28 uses command filters to accommodate magnitude, rate and bandwidth constraints on intermediate states and actuator signals. An additional advantage of this method is that in stead of tedious analytic computations, the virtual control signal's derivatives can now be acquired by command filters.

The paper is outlined as follows. First, dynamic modelling of the UAV via Kane's method is discussed in Section 2. A review of constrained backstepping method is presented in Section 3. In Section 4 the trajectory control is derived and the control of the morphing wings is presented in Section 5. Simulation examples are shown in Section 7. Finally, conclusions are given in Section 8.

https://doi.org/10.1017/S000192400000943X Published online by Cambridge University Press

2.0 ASYMMETRIC VARIABLE SWEEP UAV MODELLING

The purpose of this section is to build a multi-body dynamic model of an asymmetric variable sweep UAV based on Kane's method.

Consider the variable sweep UAV system Γ in Fig. 1, which can be treated as a multi-body system composed of three major parts: the left wing W_l, the right wing W_r and the fuselage FL. Wings are hinged to FL at O_1, O_2 by electric motors or other kind of actuators that provide torques, allowing wing sweep angles H_l, H_r to change independently. Wing dihedral angle is assumed to be zero and the wind field around the model is assumed to be static. CG (centre of gravity) of Γ, FL, W_l and W_r are O, O_f, O_l and O_r respectively.

2.1 Preliminary knowledge

Since wings and fuselage are hinged together, system Γ is subject to two configuration constraints:

1. Distances between $O_1(O_2)$ and any particle belonging to W_l (W_r) are constant.
2. The angle between $B_{\vec{z}}$ which is the unit vector along body co-ordinate system $\{B\}$'s z axis, and the velocity vector of any particle belonging to W_l (W_r) is constant. (Since the wing dihedral angle is assumed to be zero, this angle would be 90 degrees.)

Choose generalised co-ordinates (x, y, z, ϕ, θ, ψ, H_l, H_r): (x, y, z) is the co-ordinate of O_f in the earth co-ordinate system $\{I\}$, ϕ is the roll angle, θ is the pitch angle, ψ is the yaw angle, H_l is the sweep angle of the left wing and H_r is the sweep angle of the right wing.

Since the position of system's CG O varies with different wing sweep angles, here we choose the coordinate of O_f as generalised co-ordinates rather than O's co-ordinate. Accordingly, the origin of body axes co-ordinate system is also chosen as O_f. Every assignment of values to these quantities and time t corresponds with a definite admissible configuration of Γ in $\{I\}$.

Define generalised speeds (u, v, w, p, q, r, η_l, η_r), where (u, v, w) is the airspeed $\vec{V}$ expressed in $\{B\}$, (p, q, r) is the angular velocity expressed in $\{B\}$, η_l and η_r are time derivatives of H_l and H_r, respectively. We have

$$\begin{cases} \begin{bmatrix} u & v & w \end{bmatrix}^T = {}_I^B R \begin{bmatrix} \dot{x} & \dot{y} & \dot{z} \end{bmatrix}^T, \\ \begin{bmatrix} p & q & r \end{bmatrix}^T = Q^{-1} \begin{bmatrix} \dot{\phi} & \dot{\theta} & \dot{\psi} \end{bmatrix}^T, \\ \begin{bmatrix} \eta_l & \eta_r \end{bmatrix}^T = \begin{bmatrix} \dot{H}_l & \dot{H}_r \end{bmatrix} \end{cases} \quad \ldots (1)$$

where ${}_I^B R$ is the rotation matrix from $\{I\}$ to $\{B\}$, Q is the matrix relates $[p\ q\ r\ ]^T$ to $[\dot{\phi}\ \dot{\theta}\ \dot{\psi}\ ]^T$.

Equation (1) is called the kinematical differential equations for Γ in S_g. It can be solved uniquely for ($\dot{x}$, $\dot{y}$, $\dot{z}$, $\dot{\phi}$, $\dot{\theta}$, $\dot{\psi}$, $\dot{H}_l$, $\dot{H}_r$).

Based on generalised co-ordinates and generalised speeds defined above, the angular velocity of FL and the velocity of O_f in $\{I\}$ can be given by

$$\vec{\Omega}_f = {}_B^I \mathcal{R} \begin{bmatrix} p \\ q \\ r \end{bmatrix}, \vec{V}_{Of} = {}_B^I \mathcal{R} \begin{bmatrix} u \\ v \\ w \end{bmatrix}. \quad \ldots (2)$$

According to their definitions, eight partial angular velocities of FL are:

https://doi.org/10.1017/S000192400000943X Published online by Cambridge University Press

$$\vec{\omega}_1^F = \begin{bmatrix} 0 \\ 0 \\ 0 \end{bmatrix}, \vec{\omega}_2^F = \begin{bmatrix} 0 \\ 0 \\ 0 \end{bmatrix}, \vec{\omega}_3^F = \begin{bmatrix} 0 \\ 0 \\ 0 \end{bmatrix},$$

$$\vec{\omega}_4^F = \begin{bmatrix} \mathrm{Cos}\theta\,\mathrm{Cos}\psi \\ \mathrm{Cos}\theta\,\mathrm{Sin}\,\psi \\ -\mathrm{Sin}\,\theta \end{bmatrix},$$

$$\vec{\omega}_5^F = \begin{bmatrix} \mathrm{Sin}\theta\,\mathrm{Cos}\psi\,\mathrm{Sin}\phi - \mathrm{Sin}\psi\,\mathrm{Cos}\phi \\ \mathrm{Sin}\theta\,\mathrm{Sin}\psi\,\mathrm{Sin}\phi + \mathrm{Cos}\psi\,\mathrm{Cos}\phi \\ \mathrm{Cos}\theta\,\mathrm{Sin}\phi \end{bmatrix}, \quad \ldots (3)$$

$$\vec{\omega}_6^F = \begin{bmatrix} \mathrm{Sin}\theta\,\mathrm{Cos}\psi\,\mathrm{Cos}\phi + \mathrm{Sin}\psi\,\mathrm{Sin}\phi \\ \mathrm{Sin}\theta\,\mathrm{Sin}\psi\,\mathrm{Cos}\phi - \mathrm{Cos}\psi\,\mathrm{Sin}\phi \\ \mathrm{Cos}\theta\,\mathrm{Cos}\phi \end{bmatrix},$$

$$\vec{\omega}_7^F = \begin{bmatrix} 0 \\ 0 \\ 0 \end{bmatrix}, \vec{\omega}_8^F = \begin{bmatrix} 0 \\ 0 \\ 0 \end{bmatrix}.$$

and eight partial velocities of O_f are

$$\vec{v}_1^F = \begin{bmatrix} \mathrm{Cos}\theta\,\mathrm{Cos}\psi \\ \mathrm{Cos}\theta\,\mathrm{Sin}\psi \\ -\mathrm{Sin}\theta \end{bmatrix},$$

$$\vec{v}_2^F = \begin{bmatrix} \mathrm{Sin}\theta\,\mathrm{Cos}\psi\,\mathrm{Sin}\phi - \mathrm{Sin}\psi\,\mathrm{Cos}\phi \\ \mathrm{Sin}\theta\,\mathrm{Sin}\psi\,\mathrm{Sin}\phi + \mathrm{Cos}\psi\,\mathrm{Cos}\phi \\ \mathrm{Cos}\theta\,\mathrm{Sin}\phi \end{bmatrix}, \quad \ldots (4)$$

$$\vec{v}_3^F = \begin{bmatrix} \mathrm{Sin}\theta\,\mathrm{Cos}\psi\,\mathrm{Cos}\phi + \mathrm{Sin}\psi\,\mathrm{Sin}\phi \\ \mathrm{Sin}\theta\,\mathrm{Sin}\psi\,\mathrm{Cos}\phi - \mathrm{Cos}\psi\,\mathrm{Sin}\phi \\ \mathrm{Cos}\theta\,\mathrm{Cos}\phi \end{bmatrix},$$

$$\vec{v}_4^F = \vec{v}_5^F = \vec{v}_6^F = \vec{v}_7^F = \vec{v}_8^F = \begin{bmatrix} 0 \\ 0 \\ 0 \end{bmatrix}.$$

Similarly, we can obtain partial angular velocities of W_l and W_r: $\vec{\omega}_1^L$, ..., $\vec{\omega}_8^L$, W_1 $\vec{\omega}_1^R$, ..., $\vec{\omega}_8^R$; partial velocities of O_l and O_r: $\vec{v}_{L1}$, ..., $\vec{v}_{L8}$, $\vec{v}_{R1}$, ..., $\vec{v}_{R8}$.

2.2 Generalised active forces

All contact and distance forces acting on fuselage *FL* are equivalent to a couple of torque $\vec{T}_f$ and a force $\vec{R}_f$ whose line of action passes through O_f. Except for torques $\vec{T}_1$ and $\vec{T}_r$ provided by motors set on O_1 and O_2, interaction forces between wings and fuselage are not counted in since they are not contributing to system generalised forces. Drag force of the horizontal tail has little influence and is normally neglected. Therefore:

https://doi.org/10.1017/S000192400000943X Published online by Cambridge University Press

$$\vec{R}_f = \vec{G}_f + \vec{F}_B + \vec{L}_t + \vec{Y}_t + \vec{D}_f, \quad \ldots (5)$$

$$\vec{T}_f = \vec{F}_B \times \vec{d}_F + \vec{Y}_t \times \vec{d}_Y + \vec{L}_t \times \vec{d}_L + \vec{D}_f \times \vec{d}_D + \vec{T}_l + \vec{T}_r. \quad \ldots (6)$$

where $\vec{G}_f$ is the gravity of FL, $\vec{F}_B$ is the thrust force of aircraft engines, $\vec{L}_t$ is the lift force of the horizontal tail, $\vec{Y}_t$ is the aerodynamic force of the rudder, $\vec{D}_f$ is the aircraft zero lift drag, $\vec{d}_F$, $\vec{d}_Y$, $\vec{d}_L$, $\vec{d}_D$ are position vectors from O_f to any point on the line of action of corresponding forces.

Based on Equation (3), Equation (4), Equation (5) and Equation (6), the contribution of this set of forces to the generalised active force F_j for Γ in S_g is given by

$$F_{fj} = \vec{\omega}_j^F \cdot \vec{T}_f + \vec{v}_j^F \cdot \vec{R}_f, \quad j = 1,...,8. \quad \ldots (7)$$

Similarly, all forces acting on the left wing W_1 are equivalent to a couple of torque $\vec{T}_{wl}$ and a force $\vec{R}_{wl}$, while all forces acting on the right wing Wr are equivalent to a couple of torque $\vec{T}_{wr}$ and a force $\vec{R}_{wr}$. Again, only the torque provided by motors set on O_1 and O_2 are count in for interaction forces. The contribution of these two sets of forces to the generalised active force F_j are given by

$$F_{lj} = \vec{\omega}_j^L \cdot \vec{T}_{wl} + \vec{v}_j^L \cdot \vec{R}_{wl}, \quad j = 1,...,8, \quad \ldots (8)$$

$$F_{rj} = \vec{\omega}_j^R \cdot \vec{T}_{wr} + \vec{v}_j^R \cdot \vec{R}_{wr}, \quad j = 1,...,8. \quad \ldots (9)$$

Consequently, we obtain generalised active forces F_j for Γ in $\{I\}$

$$F_j = F_{fj} + F_{1j} + F_{rj}, j = 1, ..., 8. \quad \ldots (10)$$

Besides, the relationship between the lift force $\vec{L}_w$ and drag force $\vec{D}_w$ of wings can be written as

$$\left|\vec{D}_w\right| = k_L \cdot \left|\vec{L}_w\right|. \quad \ldots (11)$$

where $k_L = C_D/C_L$, C_D is the drag coefficient and C_L is the lift coefficient of a single wing respectively. This relationship can be used to simplify the form of Equation (10) during analysing.

2.3 Generalised inertia forces

The inertia force and inertia torque for rigid body FL in $\{I\}$ can be written as

$$\vec{R}_f^* = -M_f \cdot \vec{a}_{Of} \quad \ldots (12)$$

$$\vec{T}_f^* = -\vec{\alpha}_f \cdot \overleftrightarrow{I}_f - \vec{\Omega}_f \times \overleftrightarrow{I}_f \cdot \vec{\Omega}_f. \quad \ldots (13)$$

where M_f is the mass of FL, $\vec{a}_{Of}$ is the acceleration of O_f, $\overleftrightarrow{I}_f$ is the central inertia dyadic of FL, $\vec{\alpha}_f$ and $\vec{\Omega}_f$ are the angular acceleration and the angular velocity of FL in S_g, respectively.

Based on Equation (3), Equation (4), Equation (12) and Equation (13), the contribution of all inertia forces of FL to generalised inertia forces of Γ in $\{I\}$ is given by

https://doi.org/10.1017/S000192400000943X Published online by Cambridge University Press

$$F_{fj}^{*} = \vec{\omega}_j^F \cdot \vec{T}_f^{*} + \vec{v}_j^F \cdot \vec{R}_f^{*}, \quad j = 1,...,8. \qquad \ldots (14)$$

Similarly, we can obtain the inertia force $\vec{R}_l^{*}$ and inertia torque $\vec{T}_l^{*}$ for W_1; the inertia force $\vec{R}_r^{*}$ and inertia torque $\vec{T}_r^{*}$ for W_r. Their contributions to generalised inertia forces are F_{lj} (j = 1, ...,8), F_{rj}^{*} (j = 1, ..., 8) respectively.

Therefore, generalised inertia forces F_j^{*} for Γ in $\{I\}$ can be given by

$$F_j^{*} = F_{fj}^{*} + F_{lj}^{*} + F_{rj}^{*}, \quad j = 1,...,8. \qquad \ldots (15)$$

2.4 Kane's dynamic equations

Since all generalised active forces and generalised iner- tia forces of the variable UAV system Γ in $\{I\}$ have been achieved in Equation (10) and Equation (15), we can present Kane's dynamic equation for Γ in $\{I\}$ as

$$F_j + F_j^{*} = 0, j = 1, ...8. \qquad \ldots (16)$$

Combining Equation (1) with Equation (16) and employing the relationship in Equation (11), the multi-body dynamic model of 4 Γ in $\{I\}$ can be presented as

$$\begin{cases} \begin{bmatrix} u & v & w \end{bmatrix}^T = {}_I^B\mathscr{R} \begin{bmatrix} \dot{x} & \dot{y} & \dot{z} \end{bmatrix}^T, \\ \begin{bmatrix} p & q & r \end{bmatrix}^T = \mathscr{Q}^{-1} \begin{bmatrix} \dot{\phi} & \dot{\theta} & \dot{\psi} \end{bmatrix}^T, \\ \begin{bmatrix} \eta_l & \eta_r \end{bmatrix}^T = \begin{bmatrix} \dot{\mathrm{H}}_l & \dot{\mathrm{H}}_r \end{bmatrix}^T, \\ J_F F_B + J_A \begin{bmatrix} L_{wl} \\ L_{wr} \\ L_t \\ Y_t \\ D_f \end{bmatrix} + J_T \begin{bmatrix} T_l \\ T_r \end{bmatrix} + E_G \begin{bmatrix} G_f \\ G_w \end{bmatrix} = \\ K_V \begin{bmatrix} \dot{u} \\ \dot{v} \\ \dot{w} \end{bmatrix} + K_\Omega \begin{bmatrix} \dot{p} \\ \dot{q} \\ \dot{r} \end{bmatrix} + K_\eta \begin{bmatrix} \dot{\eta}_l \\ \dot{\eta}_r \end{bmatrix} + N. \end{cases} \qquad \ldots (17)$$

where J_F, J_A, J_T, E_G, K_V, K_Ω and K_η are, respectively, 8×1, 8×5, 8×2, 8×2, 8×3, 8×3, and 8×2 coefficient matrices, whose terms are composed of model characteristics and triangle functions of θ , ψ, ϕ , H_l , H_r, attack angle α and sideslip angle β ; **N** is a 8×1 matrix which contains cross terms of generalised speeds; F_B, L_t, Y_t, D_f, G_f, T_l and T_r are norms of $\vec{F}_B$, $\vec{L}_t$, $\vec{Y}_t$, $\vec{D}_f$, $\vec{G}_f$, $\vec{T}_l$ and $\vec{T}_r$, respectively; G_w, L_{wl} and L_{wr} are norms of wing gravity $\vec{G}_w$, the lift force of left wing $\vec{L}_{wl}$ and the lift force of right wing $\vec{L}_{wr}$, respectively.

Equation (17) contains all kinematic and dynamic equations of multi-body system Γ. Along with the influence of the asymmetric variable sweep wing to the entire UAV system, dynamic equations of the morphing wings themselves are also included. However, as the asymmetric variable sweep mechanism is mainly treated as a torque-provider, it does not play a key role in guidance and navigation. For simplicity, guidance and navigation equations contained in Ref. 23 are used in trajectory control design, while Kane's equations are used in attitude and wing sweep control design.

https://doi.org/10.1017/S000192400000943X Published online by Cambridge University Press

3.0 STABILITY RESULTS REVIEW

For a nonlinear system of lower-triangular form such as

$$\begin{cases} \dot{x} = P(x) + Q(x)y, \\ \dot{y} = F(x,y) + G(x,y)U. \end{cases} \quad \ldots (18)$$

where $P, Q : R^n \to R^n$, $F, G : R^n \times R^n \to R^n$ are smooth functions in the domain of definition and G, Q are invertible. The control target is to make x track a desired bounded continuous differentiable signal x^d with control U. Backstepping method is applied by first considering y as the virtual control of x, the error between y and its desired value is rendered to zero via a control Lyapunov function then to acquire global stability.

A standard procedure starts with defining the tracking error $\xi = x - x^d$. Choose a virtual control $\rho(x) = Q^{-1}[-k_\xi - P + \dot{x}_d]$, where $k > 0$ and define $\mu = y - \rho(x)$. Equation (18) can be rewritten as

$$\begin{cases} \dot{\xi} = P + Q(\mu + \rho) - \dot{x}^d, \\ \dot{\mu} = F + GU - \dot{\rho}. \end{cases} \quad \ldots (19)$$

Use $V = {}^1/_2 \xi^T \xi + {}^1/_{2\mu} T\mu$ as a Lyapunov function candidate and its derivative is

$$\begin{aligned} \dot{V} &= -k\xi^T\xi + \mu^T(Q^T\xi + F + GU - \dot{\rho}) \\ &\le -k\|\xi\|^2 + \mu^T(Q^T\xi + F + GU - \dot{\rho}). \end{aligned} \quad \ldots (20)$$

which can be rendered negative definite by control law

$$U = -G - 1(k\mu + Q^T\xi + F - \dot{\rho}). \quad \ldots (21)$$

For an ideal system with no physical constraints, the recursive design procedure ends here. However, for a real system such as UAV that is bounded by magnitude, rate and bandwidth constraints on states and actuator signals, the former presented design has not taken these into account. When the control signal demanded by the backstepping controller is too aggressive to be generated by the actuators, stability can no longer be guaranteed and the saturation may even cause physical damage to the UAV. Another drawback of the standard backstepping is that when applied to a large system, the analytic calculation of the virtual control derivatives could be quite tedious and time consuming.

To eliminate these drawbacks, command filters are used and extend the standard backstepping to so-called constrained backstepping method[25-28]. With saturation functions contained in the command filters, the inputs of the filters are desired (virtual) control signals, while the outputs are magnitude, rate and bandwidth limited actual signals and their derivatives.

One such filter can be defined as

$$\begin{aligned} \begin{bmatrix} \dot{q}_1 \\ \dot{q}_2 \end{bmatrix} &= \begin{bmatrix} q_2 \\ 2\varsigma\omega_n \left(S_R \left\{ \frac{\omega_n^2}{2\varsigma\omega_n} \left[S_M\left(x_c^0\right) - q_1 \right] \right\} - q_2 \right) \end{bmatrix}, \\ \begin{bmatrix} x_c \\ \dot{x}_c \end{bmatrix} &= \begin{bmatrix} q_1 \\ q_2 \end{bmatrix}. \end{aligned} \quad \ldots (22)$$

https://doi.org/10.1017/S000192400000943X Published online by Cambridge University Press

where x_c^0 is the input and x_c is the magnitude, rate and bandwidth limited output. Magnitude and rate limit functions S_M and S_R are defined similarly as

$$S_M(x) = \begin{cases} M & if\ x \geq M, \\ x & if\ |x| < M, \\ -M & if\ x \leq -M. \end{cases} \quad \ldots (23)$$

Note that $\dot{x}_c$ is computed without differentiation. This filter ensures that the output command signal and its derivative stay in the operating envelope defined by S_M and S_R.

In the absence of constraints, which means M and R are infinitely large and the filter always stays in the linear range of S_M and S_R, the transfer function of Equation (22) turns out to be

$$\frac{x_c(s)}{x_c^0(s)} = \frac{\omega_n^2}{s^2 + 2\varsigma\omega_n s + \omega_n^2}. \quad \ldots (24)$$

We can see that the error $|x_c - x_c^0|$ can be made arbitrarily small by selecting ω_n sufficiently larger than the band-width of x_c^0. If M and R are bounded and command limits are in effect, $|x_c - x_c^0|$ would be bounded as long as the input signal x_c^0 is bounded.

Now the stability results of system Equation (18) with physical constraints can be summarised as the following theorem.

Theorem 1: For system Equation (18), the actual (virtual) control signals ${}^F\rho$, ${}^FU$ are given by command filter Equation (22). If physical constraints on states and control signals are not in effect, the closed-loop system would be asymptotically stable with tracking errors ξ and μ. If physical constraints are in effect, the closed-loop system can still be made stable with modified tracking errors $\bar{\xi}$ and $\bar{\mu}$ which are defined subsequently, and the original tracking errors are bounded as

$$\begin{aligned} \left\| \begin{matrix} \xi(t) \\ \mu(t) \end{matrix} \right\| &\leq e^{-ct} \left\| \begin{matrix} \xi(0) \\ \mu(0) \end{matrix} \right\| \\ &+ \delta \sqrt{\frac{1 - e^{-2ct}}{4c}} \left(\sup_{\tau \in [0,t]} \left\| \begin{matrix} Q({}^F\rho - \rho) \\ G({}^FU - U) \end{matrix} \right\| \right). \end{aligned} \quad \ldots (25)$$

Proof: Since the actual (virtual) control inputs are ${}^F\rho$ and ${}^FU$, the filtered versions of ρ and U, the Lyapunove function candidate V's derivative along the closed loop system is now

$$\begin{aligned} \dot{V} &= -k_1 \xi^T \xi - k_2 \mu^T \mu + \xi^T Q({}^F\rho - \rho) + \mu^T G({}^FU - U) \\ &\leq -(k_1 - \frac{1}{2\delta_1^{\,2}}) \|\xi\|^2 - (k_2 - \frac{1}{2\delta_2^{\,2}}) \|\mu\|^2 + \frac{\delta_1^{\,2}}{2} \left\| Q({}^F\rho - \rho) \right\|^2 + \frac{\delta_2^{\,2}}{2} \left\| G({}^FU - U) \right\|^2 \\ &= -c_1 \|\xi\|^2 - c_2 \|\mu\|^2 + \frac{\delta_1^{\,2}}{2} \left\| Q({}^F\rho - \rho) \right\|^2 + \frac{\delta_2^{\,2}}{2} \left\| G({}^FU - U) \right\|^2 \\ &\leq -cV + \frac{\delta^2}{2} \left(\left\| Q({}^F\rho - \rho) \right\|^2 + \left\| G({}^FU - U) \right\|^2 \right) \end{aligned} \quad \ldots (26)$$

where $\delta_1, \delta_2 > 0$, $\delta \stackrel{\Delta}{=} \max\{\delta_1, \delta_2\}$: $c_1\Delta = k_1 - \frac{1}{2\delta_1^{\,2}}, c_2\Delta = k_2 - \frac{1}{2\delta_2^{\,2}}; c_1, c_2 > 0, c\Delta = \min\{c_1, c_2\}$

It is clear that if physical constraint on states and control signals are not in effect, $({}^F\rho - \rho)$ and

https://doi.org/10.1017/S000192400000943X Published online by Cambridge University Press

($^{F}U - U$) can be made arbitrarily small by selecting ω_n large enough. Thus $\dot{V}$ can still be made negative definite and the convergence of tracking errors is guaranteed in the sense of Lyapunov.

If physical constraints are in effect, which means that the requested tracking signal is too aggressive and the required (virtual) controls are pushed off limits, the goal is then to maintain stability of the system and keep ρ and U in their safe operating envelope defined a priori.

Modify the definition of tracking errors as

$$\begin{aligned} \bar{\xi} &= \xi - \xi_1, \\ \bar{\mu} &= \mu - \zeta_2. \end{aligned} \quad \ldots (27)$$

where ζ_1 and ζ_2 satisfy

$$\begin{aligned} \dot{\zeta}_1 &= -k_1\zeta_1 + Q(^{F}\rho - \rho), \\ \dot{\zeta}_2 &= -k_2\zeta_2 + G(^{F}U - U). \end{aligned} \quad \ldots (28)$$

Now the modified Lyapunov function is $V = {}^1/_2\,\bar{\xi}^T\bar{\xi} + 12\,\bar{\mu}^T\bar{\mu}$ and its derivative is

$$\begin{aligned} \dot{V} &= -k_1\bar{\xi}^T\bar{\xi} - k_2\bar{\mu}^T\bar{\mu} \\ &\le -k_1\left\|\bar{\xi}\right\|^2 - k_2\left\|\bar{\mu}\right\|^2. \end{aligned} \quad \ldots (29)$$

We can see from Equation (29) that $\dot{V}$ can still be made negative definite with modified tracking errors $\bar{\xi}$ and $\bar{\mu}$, which means that $\bar{\xi}$ and $\bar{\mu}$ still converge to zero when physical constraints are in effect.

For the original tracking errors ξ and μ, it is clear that they will not be zero since the desired (virtual) control signals are impossible to be implemented under physical constraints. However, they can still remain bounded depending on the filter errors. Multiplying both sides of Equation (26) by e^{-2ct} and calculating their integrals on [0, t], yields

$$\begin{aligned} V(t) &\le e^{-2ct}V(0) + \frac{\delta^2}{2}\int_0^t e^{-2c(t-\tau)}\left(\left\|Q(^{F}\rho - \rho)\right\|^2 + \left\|G(^{F}U - U)\right\|^2\right)d\tau \\ &\le e^{-2ct}V(0) + \delta^2\frac{1-e^{-2ct}}{4c}\sup_{\tau\in[0,t]}\left(\left\|Q(^{F}\rho - \rho)\right\|^2 + \left\|G(^{F}U - U)\right\|^2\right), \\ &\forall t \ge 0. \end{aligned} \quad \ldots (30)$$

Calculating the square root of both sides of Equation (30) and employing the definition of V, we can obtain the inequality Equation (25)

Equation (25) shows that the original tracking errors would be bounded as long as the filter errors are bounded.

Remark 1: Note that ζ_1 and ζ_2 would converge to zero if physical constraints are not in effect, in that case $\bar{\xi}$ converges to ξ, $\bar{\mu}$ converges to μ.

4.0 TRAJECTORY TRACKING CONTROL DESIGN

In this section, we present an integrated guidance and control design with constrained back-stepping method. The control objective is to make the UAV asymptotically track the desired smooth inertial trajectory $P^d = [x^d, y^d, z^d]^T$ with position states $P = [x, y, z]^T$. Magnitude, rate and band width constraints on states and actuator signals are accommodated by command filters defined as Equation (22). Furthermore, the sideslip angle β is kept at zero to ensure co-ordinated turning.

https://doi.org/10.1017/S000192400000943X Published online by Cambridge University Press

As mentioned before, the roll control is done by asymmetric wing sweep morphing instead of aileron, thus the available controls are the engine thrust F_B, the control-surface deflections δ_e, δ_r and the differential wing sweep angle morphing δ_η. The constrained back-stepping control design is then done in four feedback steps.

4.1 Inertial position control

Let position states be $X_0 = P = [x, y, z]^T$, and the desired trajectory satisfies

$$X_0^d = \dot{P}^d = \begin{bmatrix} V^d \mathrm{Cos}\gamma^d \mathrm{Cos}\chi^d \\ V^d \mathrm{Cos}\gamma^d \mathrm{Sin}\chi^d \\ -V^d \mathrm{Sin}\gamma^d \end{bmatrix}. \quad \ldots (31)$$

where V^d is the desired airspeed, γ^d and χ^d are desired flight path angles.

The error vector is defined by transforming the tracking errors expressed in the inertial frame $\{I\}$ to a new reference frame that is fixed to the UAV and aligned with the horizontal component of $\vec{V}$[25]

$$e_0 \Delta = \begin{bmatrix} e_{01} \\ e_{02} \\ e_{03} \end{bmatrix} = \begin{bmatrix} \mathrm{Cos}\chi & \mathrm{Sin}\chi & 0 \\ -\mathrm{Sin}\chi & \mathrm{Cos}\chi & 0 \\ 0 & 0 & 1 \end{bmatrix} (X_0 - X_0^d). \quad \ldots (32)$$

Differentiating Equation (32) gives

$$\dot{e}_0 = \begin{bmatrix} V\mathrm{Cos}\gamma + e_{02}\dot{\chi} - V^d \mathrm{Cos}\gamma^d \mathrm{Cos}(\chi - \chi^d) \\ -e_{01}\dot{\chi} + V^d \mathrm{Cos}\gamma^d \mathrm{Sin}(\chi - \chi^d) \\ -V\mathrm{Sin}\gamma + V^d \mathrm{Sin}\gamma^d \end{bmatrix}. \quad \ldots (33)$$

From Equation (33) we can see that e_{01} and e_{03} can be regulated to zero by selecting virtual controls

$$\tilde{V} = \frac{V^d \mathrm{Cos}\gamma^d \mathrm{Cos}(\chi - \chi^d) - c_{01} e_{01}}{\mathrm{Cos}\gamma}, \quad \ldots (34)$$

$$\tilde{\gamma} = \mathrm{Arcsin}\left(\frac{c_{03} e_{03} + V^d \mathrm{Sin}\gamma^d}{V} \right), \quad -\frac{\pi}{2} < \tilde{\gamma} < \frac{\pi}{2}.$$

where $c_{01}, c_{03} > 0$ are control gains.

To accommodate physical constraints on system states and controls and avoid tedious derivatives calculation, the actual implementable virtual control signals ${}^F V$ and ${}^F\gamma$ as well as their derivatives ${}^F\dot{V}$ and ${}^F\dot{\gamma}$ are given by command filters Equation (22). It ensures that the tracking error con- verges to zero when physical constrains are not in effect, and maintains system stability when physical constraints are in effect with modified tracking errors.

Note that e_{02}'s control design will be left to the next design step.

4.2 Airspeed and flight path angle control

The objective of this design step is to make V and γ converge to their desired values that have been given as ${}^F V$ and ${}^F\gamma$ in the previous section. Moreover, the heading angle χ must track its desired value χ^d and have e_{02} regulated to zero in the meantime. The chosen (virtual) controls are engine thrust F_B, the aerodynamic angles μ and α.

https://doi.org/10.1017/S000192400000943X Published online by Cambridge University Press

Define $X_1 = [\mathrm{V}\ \ \chi\ \ \gamma]^T$, $X_1^d = [{}^F V\ \ \chi \mathrm{d}\ \ {}^F\gamma]^T$, and $X_2 = [\mu\ \ \alpha\ \ \beta]^T$, thus the relevant equations of motion can be given by

$$\dot{X}_1 = A_1 F_1(X) + B_1 G_1(X, X_2) + H_1(X). \quad \ldots (35)$$

$$A_1 = \frac{1}{mV}\begin{bmatrix} 0 & 0 & -V \\ 0 & \dfrac{\mathrm{Cos}(\mu)}{\mathrm{Cos}(\gamma)} & 0 \\ 0 & -\mathrm{Sin}(\mu) & 0 \end{bmatrix},$$

$$B_1 = \frac{1}{mV}\begin{bmatrix} V\mathrm{Cos}(\alpha)\mathrm{Cos}(\beta) & 0 & 0 \\ 0 & \dfrac{1}{\mathrm{Cos}(\gamma)} & 0 \\ 0 & 0 & 1 \end{bmatrix}, \quad \ldots (36)$$

$$H_1 = \begin{bmatrix} -g\mathrm{Sin}(\gamma) \\ \dfrac{F_B}{mV\mathrm{Cos}(\gamma)}\mathrm{Cos}(\alpha)\mathrm{Sin}(\beta)\mathrm{Cos}(\mu) \\ \dfrac{F_B}{mV}\mathrm{Cos}(\alpha)\mathrm{Sin}(\beta)\mathrm{Sin}(\mu) - \dfrac{g}{V}\mathrm{Cos}(\gamma) \end{bmatrix}.$$

are known matrix-valued functions and

$$F_1 = \begin{bmatrix} L(X) \\ Y(X) \\ D(X) \end{bmatrix}, G_1 = \begin{bmatrix} F_B \\ \big(L(X) + F_B\mathrm{Sin}(\alpha)\big)\mathrm{Sin}(\mu) \\ \big(L(X) + F_B\mathrm{Sin}(\alpha)\big)\mathrm{Cos}(\mu) \end{bmatrix}. \quad \ldots (37)$$

are functions that contain lift, side, and drag forces $L = -L_{wl} - L_{wr}$, $Y = Y_t$, $D = -(D_f + k_L L_{wl} + k_L L_{wr})$.

There are several ways of acquiring the value of these aerodynamic forces. One way is to estimate them through neural network online approximation[25,26]. The most often used way, however, is done by applying a nominal model of these forces which is acquired through wind tun- nel testing or flight experiment. For a typical type of UAV, the second way is usually more reliable. We can decompose the lift force as

$$L(X) = L_0(X) + L_\alpha(X)\alpha. \quad \ldots (38)$$

and rewrite G_1 as

$$G_1 = \begin{bmatrix} F_B \\ \big(L_0(X) + L_\alpha(X)\alpha + F_B\mathrm{Sin}(\alpha)\big)\mathrm{Sin}(\mu) \\ \big(L_0(X) + L_\alpha(X)\alpha + F_B\mathrm{Sin}(\alpha)\big)\mathrm{Cos}(\mu) \end{bmatrix}$$
$$\Delta = \begin{bmatrix} F_B & G_{1y} & G_{1z} \end{bmatrix}^T. \quad \ldots (39)$$

Defining the tracking error

$$e_1 = [e_{11}\ e_{12}\ e_{13}]^T = X_1 - X_1^d. \quad \ldots (40)$$

https://doi.org/10.1017/S000192400000943X Published online by Cambridge University Press

and differentiating Equation (40) gives

$$\dot{e}_1 = A_1 F_1 + B_1 \mathrm{G}_1 + H_1 - \dot{X}_1^d . \quad \ldots (41)$$

Now we can use G_1 in Equation (39) as the virtual control to regulate e_1 and e_{02} to zero by choosing

$$\tilde{G}_1 = \begin{bmatrix} F_B \\ \tilde{G}_{1y} \\ \tilde{G}_{1z} \end{bmatrix} = B_1^{-1}\left(\begin{bmatrix} -c_{11}e_{11} \\ -V^d \mathrm{Cos}(\gamma^d)(c_{02}e_{02} + c_{12}\mathrm{Sin}(e_{12})) \\ -c_{13}e_{13} \end{bmatrix} - A_1 F_1 - H_1 + \dot{X}_1^d \right). \quad \ldots (42)$$

where c_{02}, c_{11}, c_{12}, $c_{13} > 0$ are control gains.

From Equation (42) we acquire the control signal F_B

$$F_B = \frac{-mc_{11}e_{11} + D + mg\mathrm{Sin}(\gamma) + m\dot{X}_1^d}{\mathrm{Cos}(\alpha)\mathrm{Cos}(\beta)}. \quad \ldots (43)$$

as well as the virtual control signals

$$\tilde{\alpha} = \frac{\sqrt{\tilde{G}_{1y}^2 + \tilde{G}_{1z}^2} - L_0 - F_B \mathrm{Sin}(\alpha)}{L_\alpha}. \quad \ldots (44)$$

and

$$\tilde{\mu} = \begin{cases} \mathrm{Arctan}\left(\tilde{G}_{1y}/\tilde{G}_{1z}\right) & if\ \tilde{G}_{1z} > 0 \\ \mathrm{Arctan}\left(\tilde{G}_{1y}/\tilde{G}_{1z}\right) + \pi & if\ \tilde{G}_{1z} < 0, \tilde{G}_{1y} \geq 0 \\ \mathrm{Arctan}\left(\tilde{G}_{1y}/\tilde{G}_{1z}\right) - \pi & if\ \tilde{G}_{1z} < 0, \tilde{G}_{1y} < 0 \\ \pi/2 & if\ \tilde{G}_{1z} = 0, \tilde{G}_{1y} > 0 \\ -\pi/2 & if\ \tilde{G}_{1z} = 0, \tilde{G}_{1y} < 0 \end{cases} \quad \ldots (45)$$

Note that the virtual control $\tilde{\mu}$ is undefined when $\tilde{G}_{1z}$ and $\tilde{G}_{1y}$ are both zero, which would only happen in the rarely case of zero or negative attack angles. This situation should be avoided by filtering the α signal with such constraint.

Again the actual implementable virtual control signals ${}^F\alpha$ and ${}^F\mu$ as well as their derivatives ${}^F\dot{\alpha}$ and ${}^F\dot{\mu}$ are given by command filter Equation (22). With physical constraints on thrust F_B in effect, it should also be filtered.

4.3 Aerodynamic angles control

The objective of this design step is to make aerodynamic angles μ and α track their desired values given as ${}^F\mu$ and ${}^F\alpha$. Besides, the sideslip angle β should be kept zero. The chosen virtual control are angular rates p, q and r.

Define $X_2 = [\mu\ \alpha\ \beta]^T$, $X_2^d = [{}^F\mu\ {}^F\alpha\ 0]^T$ and $X_3 = [p\ q\ r]^T$, and the relevant equations can be given by

$$\dot{X}_2 = A_2 F_1(X) + B_2(X)X_3 + H_2(X). \quad \ldots (46)$$

where

https://doi.org/10.1017/S000192400000943X Published online by Cambridge University Press

$$A_2 = \frac{1}{mV}\begin{bmatrix} \mathrm{Tan}(\beta)+\mathrm{Tan}(\gamma)\mathrm{Sin}(\mu) & \mathrm{Tan}(\gamma)\mathrm{Cos}(\mu)\mathrm{Cos}(\beta) & \mathrm{Sin}(\beta)\mathrm{Cos}(\mu)\mathrm{Tan}\gamma \\ -1/\mathrm{Cos}(\beta) & 0 & 0 \\ 0 & \mathrm{Cos}(\beta) & \mathrm{Sin}(\beta) \end{bmatrix},$$

$$B_2 = \begin{bmatrix} -\mathrm{Cos}(\alpha)\mathrm{Tan}(\beta) & 0 & \mathrm{Sin}(\alpha)/\mathrm{Cos}(\beta) \\ -\mathrm{Cos}(\alpha)\mathrm{Tan}(\beta) & 1 & -\mathrm{Sin}(\alpha)\mathrm{Tan}(\beta) \\ \mathrm{Sin}(\alpha) & 0 & -\mathrm{Cos}(\alpha) \end{bmatrix},$$

$$H_2 = \frac{1}{mV}\begin{bmatrix} [F_B(\mathrm{Sin}(\alpha)\mathrm{Tan}(\gamma)\sin(\mu)+\mathrm{Sin}(\alpha)\mathrm{Tan}(\beta)- \\ \mathrm{Cos}(\alpha)\mathrm{Sin}(\beta)\mathrm{Tan}(\gamma)\mathrm{Cos}(\mu))- \\ mg\mathrm{Tan}(\beta)\mathrm{Cos}(\gamma)\mathrm{Cos}(\mu)] \\ \frac{1}{\mathrm{Cos}(\beta)}(F_B\mathrm{Sin}(\alpha)+mg\mathrm{Cos}(\gamma)\mathrm{Cos}(\mu)) \\ -F_B\mathrm{Cos}(\alpha)\mathrm{Sin}(\beta)+mg\mathrm{Cos}(\gamma)\mathrm{Sin}(\mu) \end{bmatrix}. \quad \ldots (47)$$

Defining the tracking error

$$e_2 = X_2 - X_2^d. \quad \ldots (48)$$

and differentiating it gives

$$\dot{e}_2 = A_2F_1 + B_2X_3 + H_2 - \dot{X}_2^d. \quad \ldots (49)$$

Now the virtual control can be chosen as

$$\tilde{X}_3 = B_2^{-1}(-C_2e_2 - A_2F_1 - H_2 + \dot{X}_2^d). \quad \ldots (50)$$

where $C_2 = C_2^T > 0$ is the control gain matrix.

The actual implementable virtual control signal ${}^FX_3$ and its derivative ${}^F\dot{X}_3$ are still given by the command filter to accommodate physical constraints.

4.4 Angular rates control

Since the desired angular rates has been give in the pre- vious section as ${}^FX_3$, the objective of this design step is to [make X_3 converges to ${}^FX_3$. The control inputs are $U_\delta = [\delta_e\ \delta_\eta\ \delta_r]^T$, where δ_e is the elevator deflection, δ_r is the rudder deflection and δ_η is the differential wing sweep angle of two wings.

For a UAV capable of asymmetric variable wing sweep angle change, the differential sweep angle of two wings δ_η can be used as the roll controller as well as ailerons. To clarify this, we present the wing's lift force as Ref. 23.

$$L_{wl} = \frac{1}{2}\rho V^2\mathrm{Cos}^2(H_0 - \frac{\delta_\eta}{2})S_wC_A,$$
$$L_{wr} = \frac{1}{2}\rho V^2\mathrm{Cos}^2(H_0 + \frac{\delta_\eta}{2})S_wC_A. \quad \ldots (51)$$

thus the roll moment generated by differential wing sweep angle is

https://doi.org/10.1017/S000192400000943X Published online by Cambridge University Press

$$\vec{M}_{\eta} = \vec{r}_{wl} \times \vec{L}_{wl} + \vec{r}_{wr} \times \vec{L}_{wr}. \quad \ldots (52)$$

Neglect the influence of δ_η on the arm of forces by assuming $\left\| \vec{r}_{wl} \right\| = \left\| \vec{r}_{wr} \right\| = r_w$, and the simplified relation between UAV roll moment and δ_η can be presented as

$$\begin{aligned} M_{\eta} &= r_w \frac{1}{2} \rho V^2 S_w C_A [\mathrm{Cos}^2(\mathrm{H}_0 - \frac{\delta_\eta}{2}) - \mathrm{Cos}^2(H_0 + \frac{\delta_\eta}{2})] \\ &= r_w \frac{1}{2} \rho V^2 S_w C_A \mathrm{Sin}(2H_0) \mathrm{Sin}(\delta_\eta) \\ &\approx r_w \frac{1}{2} \rho V^2 S_w C_A \delta_\eta \mathrm{Sin}(2H_0) \end{aligned} \quad \ldots (53)$$

A control allocator needs to be designed for δ_η and the aileron to be able to co-work with each other. In this paper, we only consider the case that δ_η works alone as the UAV roll controller.

By neglecting terms equal to zero in the 4, 5 and 6 lines of Kane's dynamic equations Equation (17), we have

$$\begin{aligned} \dot{X}_3 = (K_\Omega^\Omega)^{-1} (J_A^\Omega \begin{bmatrix} L_{wl} \\ L_{wr} \\ L_t \\ Y_t \end{bmatrix} + E_G^\Omega \begin{bmatrix} G_f \\ G_w \end{bmatrix} - \\ K_V^\Omega \begin{bmatrix} \dot{u} \\ \dot{v} \\ \dot{w} \end{bmatrix} - K_\eta^\Omega \begin{bmatrix} \dot{\eta}_1 \\ \dot{\eta}_2 \end{bmatrix} - N^\Omega). \end{aligned} \quad \ldots (54)$$

which can then be rewritten as

$$\dot{X}_3 = A_3 (F_3(X, U_\delta) + B_3(X) U_\delta) + H_3(X). \quad \ldots (55)$$

$$A_3 = (K_\Omega^\Omega)^{-1},$$

$$H_3 = (K_\Omega^\Omega)^{-1} (K_V^\Omega \begin{bmatrix} \dot{u} \\ \dot{v} \\ \dot{w} \end{bmatrix} - K_\eta^\Omega \begin{bmatrix} \dot{\eta}_1 \\ \dot{\eta}_2 \end{bmatrix} - N^\Omega). \quad \ldots (56)$$

and

$$F_3(X, U_\delta) + B_3(X) U_\delta = J_A^\Omega \begin{bmatrix} L_{wl} \\ L_{wr} \\ L_t \\ Y_t \end{bmatrix} + E_G^\Omega \begin{bmatrix} G_f \\ G_w \end{bmatrix}. \quad \ldots (57)$$

Note that the right side of Equation (57) is the total inertial moment acting on the UAV. Gravity forces are included because of the change of mass distribution caused by wing sweep angle changes. It can then be rewritten as

$$J_A^\Omega \begin{bmatrix} L_{wl} \\ L_{wr} \\ L_t \\ Y_t \end{bmatrix} + E_G^\Omega \begin{bmatrix} G_f \\ G_w \end{bmatrix} = \begin{bmatrix} \bar{L} \\ \bar{M} \\ \bar{N} \end{bmatrix}. \quad \ldots (58)$$

https://doi.org/10.1017/S000192400000943X Published online by Cambridge University Press

where $\bar{L}$, $\bar{M}$ and $\bar{N}$ can be acquired through wind tunnel testing or flight experiment and be decomposed into a similar form as

$$\bar{L} = \bar{L}_0(X,U_\delta) + \bar{L}_{\delta_e}\delta_e + \bar{L}_{\delta_\eta}\delta_\eta + \bar{L}_{\delta_r}\delta_r. \quad \ldots (59)$$

Thus F_3 and B_3 can be given by

$$F_3 = \begin{bmatrix} \bar{L}_0 \\ \bar{M}_0 \\ \bar{N}_0 \end{bmatrix}, B_3 = \begin{bmatrix} \bar{L}_{\delta_e} & \bar{L}_{\delta_\eta} & \bar{L}_{\delta_r} \\ \bar{M}_{\delta_e} & \bar{M}_{\delta_\eta} & \bar{M}_{\delta_r} \\ \bar{N}_{\delta_e} & \bar{N}_{\delta_\eta} & \bar{N}_{\delta_r} \end{bmatrix}. \quad \ldots (60)$$

Now to steer X_3 to its desired value ${}^F X_3$, defining the tracking error

$$e_3 = X_3 - X_3^d \ldots \quad \ldots (61)$$

and differentiating it gives

$$\dot{e}_3 = A_3 (F_3 + B_3 \mathrm{U}_\delta) + H_3 - \dot{X}_3^d. \quad \ldots (62)$$

The control signal can then be chosen as

$$U_\delta = (A_3 B_3)^{-1} (-C_3 e_3 - A_3 F_3 - H_3 + \dot{X}_3^d). \quad \ldots (63)$$

where $C_3 = C_3^T > 0$ is the control gain matrix.

Due to the wing's own weight and the aerodynamic forces acting on it, magnitude and rate constraints of δ_η are quite obvious. Physical constraints of δ_e and δ_r are usually pre-defined as well. Thus the actual implementable control signal ${}^F U_\delta$ and its derivative ${}^F \dot{U}_\delta$ are again given by command filter Equation (22).

By now we have finished the trajectory tracking control design for the asymmetric variable sweep wing UAV via constrained backstepping method. Control signals F_B, δ_e, δ_r and δ_η are filtered to accommodate physical constraints. Note that the differential wing sweep angles of two wings $\delta\eta$ are used as the roll controller rather than ailerons.

5.0 ASYMMETRIC WING SWEEP CONTROL

Wing sweep control during flight has always been a challenging subject, especially when it is done in a asymmetric way and considered as the UAV roll controller. Aerodynamic forces and mass distribution changes caused by sweep angle variation lead to complicated coupling effects between wings and the motion of UAV. In this paper, Kane's equations are used to present a nominal model for dynamic characteristics of the asymmetric variable sweep wing, and the control design is done via constrained backstepping as follows.

Since the desired differential wing sweep angles have been given in the previous section as $H_l^d = H_0 - {}^F\delta_\eta / 2$, $H_r^d = H_0 + {}^F\delta_\eta / 2$, the control objective here is to steer wing sweep angles $H_l^0 = H_r^0 = H_0$ to their desired values. Torques T_l and T_r provided by actuators set on O_1, O_2 are chosen as the control signals.

https://doi.org/10.1017/S000192400000943X Published online by Cambridge University Press

Define

$$X_4 = \begin{bmatrix} H_l \\ H_r \end{bmatrix}, \quad X_5 = \dot{X}_4 = \begin{bmatrix} \eta_l \\ \eta_r \end{bmatrix}, \quad X_4^d = \begin{bmatrix} H_l^d \\ H_r^d \end{bmatrix}, \quad U_T = \begin{bmatrix} T_l \\ T_r \end{bmatrix}. \qquad \ldots (64)$$

Defining the error vector

$$e_4 = X_5 - X_4^d. \qquad \ldots (65)$$

and differentiating it gives

$$\dot{e}_4 = X_5 - \dot{X}_4^d \qquad \ldots (66)$$

where $\dot{X}_4^d = \begin{bmatrix} -\frac{{}^F\dot{\delta}_\eta}{2} & \frac{{}^F\dot{\delta}_\eta}{2} \end{bmatrix}^T$ is given by the command filter.

Choose the virtual control

$$\tilde{X}_5 = -C_4 e_4 + \dot{X}_4 \qquad \ldots . (67)$$

where $C_4 = C_4^T > 0$ is the control gain matrix. The actual implementable control signal ${}^FX_5$ and its derivative ${}^F\dot{X}_5$ are still given by command filter Equation (22).

Now the objective is to make X_5 track its desired value $X_5^d = {}^FX_5$, while the control signal is U_T. By neglecting terms equal to zero in the 7th and 8th lines of Kane's equations Equation (17). The dynamic model of the wings can be written as:

$$\dot{X}_5^d = B_5 U_T + H_5. \qquad \ldots (68)$$

where

$$B_5 = (K_\eta^\eta)^{-1} J_T^\eta,$$
$$H_5 = (K_\eta^\eta)^{-1}(J_A^\eta \begin{bmatrix} L_{wl} \\ L_{wr} \end{bmatrix} + E_G^\eta \begin{bmatrix} G_f \\ G_w \end{bmatrix} - K_V^\eta \begin{bmatrix} \dot{u} \\ \dot{v} \\ \dot{w} \end{bmatrix} - K_\Omega^\eta \begin{bmatrix} \dot{p} \\ \dot{q} \\ \dot{r} \end{bmatrix} - N^\eta). \qquad \ldots (69)$$

Defining the tracking error

$$e_5 = X_5 - X_5^d. \qquad \ldots (70)$$

and differentiating it gives

$$\dot{e}_5 = B_5 U_T + H_5 - \dot{X}_5^d. \qquad \ldots (71)$$

The control signal can now be chosen as

$$U_T = B_5^{-1}(-C_5 e_5 - H_5 + \dot{X}_5^d). \qquad \ldots (72)$$

https://doi.org/10.1017/S000192400000943X Published online by Cambridge University Press

where $C_5 = C_5^T > 0$ is the control gain matrix.

Considering that the actuator may have magnitude and rate limits, the actual implementable control signal ${}^F U_T$ are given by the command filter Equation 22.

6.0 STABILITY ANALYSIS

In this section the stability property of the previous designed control law is discussed in the sense of Lyapunov.

Choosing the Lyapunov function candidate

$$V = \frac{1}{2}(e_0^T e_0 + e_{11}^2 + \frac{2-2\mathrm{Cos}(e_{12})}{c_{02}} + e_{13}^2 + e_2^T e_2 + e_3^T e_3 + e_4^T e_4 + e_5^T e_5). \quad \ldots(73)$$

and differentiating it along the closed loop system gives

$$\begin{aligned}\dot{V} = & -c_{01}e_{01}^2 - c_{03}e_{03}^2 - c_{11}e_{11}^2 - V^d \mathrm{Cos}(\gamma^d)\frac{c_{12}}{c_{02}}\mathrm{Sin}^2(e_{12}) \\ & -c_{13}e_{13}^2 - e_2^T C_2 e_2 - e_3^T C_3 e_3 - e_4^T C_4 e_4 - e_5^T C_5 e_5 \\ & +e_{01}({}^F V - \tilde{V}) + e_{03}{}^F V(\mathrm{Sin}({}^F\gamma) - \mathrm{Sin}(\tilde{\gamma})) \\ & +e_1^T B_1(G_1({}^F X_2) - G_1(\tilde{X}_2)) + e_2^T B_2({}^F X_3 - \tilde{X}_3) \\ & +e_3^T A_3 B_3({}^F U_\delta - U_\delta) + e_4^T({}^F X_5 - \tilde{X}_5) \\ & +e_4^T B_5({}^F U_T - U_T).\end{aligned} \quad \ldots(74)$$

When no physical constraints are in effect, it is clear that the terms caused by command filters in Equation (74) can be made infinitely small by selecting the bandwidth of the filters sufficiently large. Thus $\dot{V}$ is negative semi-definite. Since the chosen Lyapunov function is not radially unbounded, only local stability is guaranteed. In the real flight, we only need to make $e_{12} \leq \pm \pi/2$ to ensure that the system stays in the stable zone.

If the desired trajectory is too aggressive or the control surfaces suffer from some physical damage, the magnitude and rate limits of states and controls would be in effect. In such cases, the UAV will not be able to track the original desired trajectory, $\dot{V}$ in Equation (74) will not be made negative semi-definite and the tracking error will not be regulate to zero. However, stability can still be acquired with modified tracking errors defined as

$$\begin{aligned}\bar{e}_0 &= e_0 - \varsigma_0, \dot{\varsigma}_0 = -C_0\varsigma_0 + ({}^F X_1 - \tilde{X}_1), \\ \bar{e}_1 &= e_1 - \varsigma_1, \dot{\varsigma}_1 = -C_1\varsigma_1 + B_1(G_1({}^F X_2) - G_1(\tilde{X}_2)), \\ \bar{e}_2 &= e_2 - \varsigma_2, \dot{\varsigma}_2 = -C_2\varsigma_2 + B_2({}^F X_3 - \tilde{X}_3), \\ \bar{e}_3 &= e_3 - \varsigma_3, \dot{\varsigma}_3 = -C_3\varsigma_3 + A_3B_3({}^F U_\delta - U_\delta), \\ \bar{e}_4 &= e_4 - \varsigma_4, \dot{\varsigma}_4 = -C_4\varsigma_4 + ({}^F X_5 - \tilde{X}_5), \\ \bar{e}_5 &= e_5 - \varsigma_5, \dot{\varsigma}_5 = -C_5\varsigma_5 + B_5({}^F U_T - U_T).\end{aligned} \quad \ldots(75)$$

The $\varsigma_0, \ldots, \varsigma_5$ terms in Equation (75) are actually used to remove the filter errors from original tracking errors. It is clear that the modified tracking errors would converge to zero when physical constraints are in effect. Although the original tracking error will not be zero, it can still converge into a bounded zone depending on command filters errors according to Theorem 1.

https://doi.org/10.1017/S000192400000943X Published online by Cambridge University Press

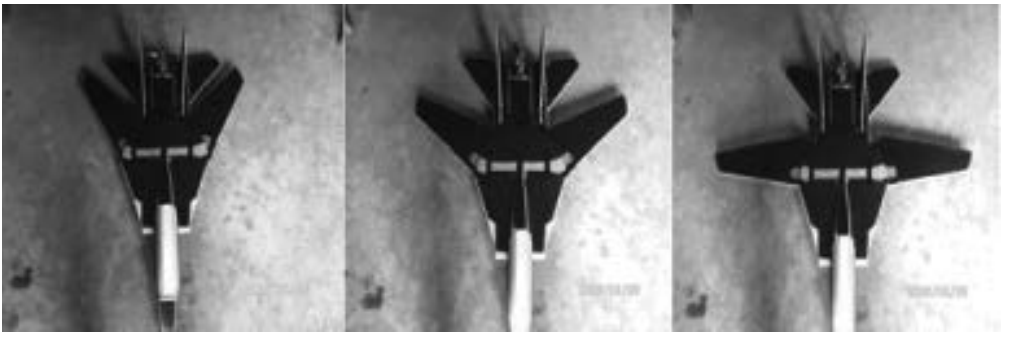


Figure 2. Variable sweep morphing UAV.

7.0 SIMULATION RESULTS

In this section we will investigate the performance of former presented control laws. Model parameters of the experiment variable sweep UAV showed in Fig. 2 can be found in Ref. 18. Although this UAV was designed to perform symmetric wing sweep angle changes, we can make use of its parameter and aerodynamic data in an asymmetric simulation as well. Command filter parameters and physical constraints of states and actuator signals are given in Table 1.

The simulation starts at the trim conditions: $h = 30$m, $V = 9{\cdot}2\text{ms}^{-1}$, and $\alpha = \theta = 0{\cdot}15$rad, where h is the altitude of the UAV and all other trim states are equal to zero. The ten initial position error vector is $[5, 15, 5]m$. The desired trajectory include two manoeuvres: the first is a straight line level flight, and the second is a helix climbing path defined as ${}^{d}/_{dt}\, P^{d} = [8\text{Cos}(0{\cdot}1)\ \text{Cos}(0{\cdot}2t),\ 8\text{Cos}(0{\cdot}1)\ \text{Sin}(0{\cdot}2t),\ -8\text{Sin}(0{\cdot}1)]$. This is a simulation of a typical UAV reconnaissance mission scenario. The control of asymmetric morphing is also simulated and we can see the different action of two wings when the UAV does different manoeuvres.

Figure 3 and Fig. 4 show that the UAV can track the reference signals very well even when the desired trajectory changes from straight line level flight into helix climbing. Flight path angles tracking are given in Fig. 5 and Fig. 6. Figure 7 shows the airspeed signal tracking in different flight stages. It can be seen from Fig. 8 that the climbing flight demands a larger thrust force than the level flight. Aerodynamic angles and attitude angles are shown in Fig. 9 and Fig. 10, respectively.

Table 1
Command filter parameters

Command variable	ωn, rad/s	Mag.limit	Rate limit
V	10	20−5m/s	5m/s^2
γ	10	±1·5rad	0·2rad/s
F_B	10	10−0N	5N/s
μ	20	±1·5rad	0·2rad/s
α	20	0·5−0·05rad	0·2rad/s
p	20	±1rad/s	–
q	20	±1rad/s	–
r	20	±1rad/s	–
δ_e	20	±0·5rad	±1rad/s
δ_r	20	±0·5rad	±1rad/s
δ_η	20	± π 12 rad	0·2rad/s

https://doi.org/10.1017/S000192400000943X Published online by Cambridge University Press

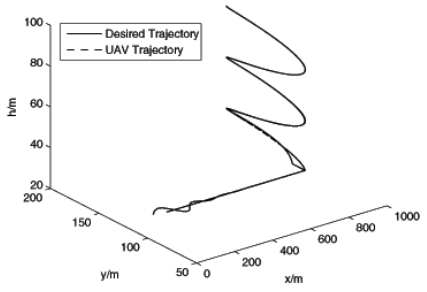


Figure 3. UAV trajectory tracking.

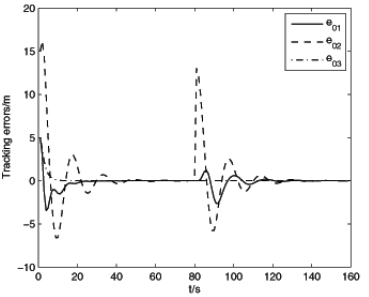


Figure 4. UAV trajectory tracking errors.

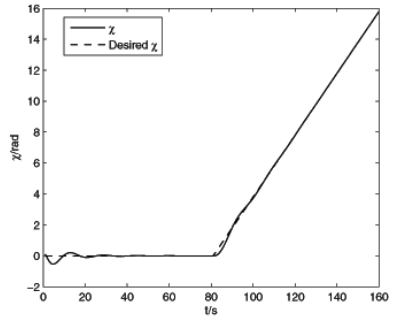


Figure 5. Flight path angle χ tracking.

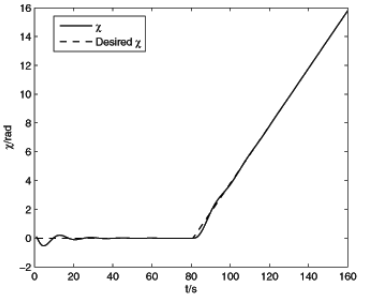


Figure 6. Flight path angle γ.

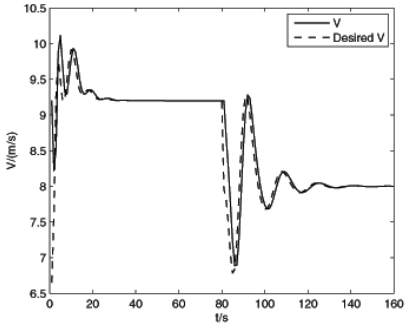


Figure 7. Airspeed *V* tracking.

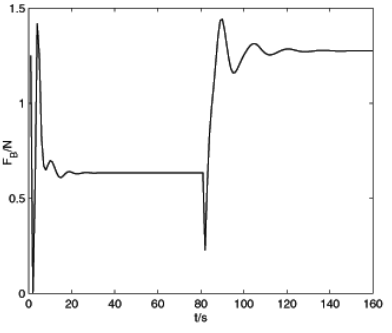


Figure 8. Thrust force.

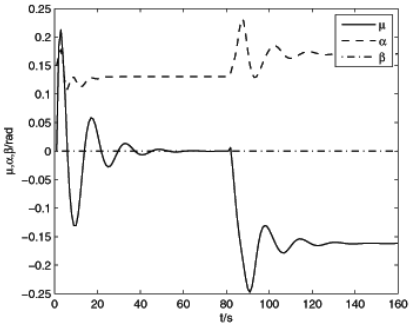


Figure 9. Aerodynamic angles.

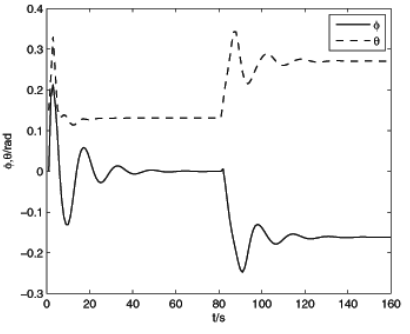


Figure 10. Attitude angles θ and ϕ .

https://doi.org/10.1017/S000192400000943X Published online by Cambridge University Press

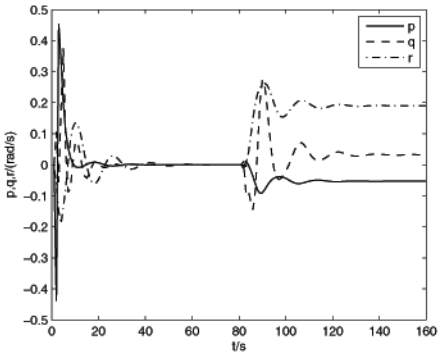


Figure 11. Angular rates.

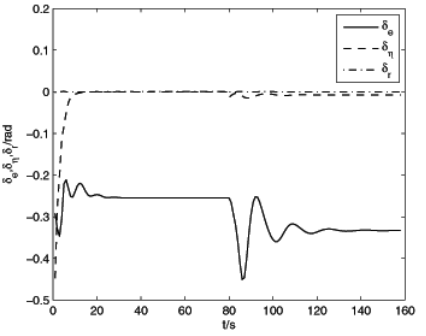


Figure 12. Control surface deflections and differential wing sweep angle.

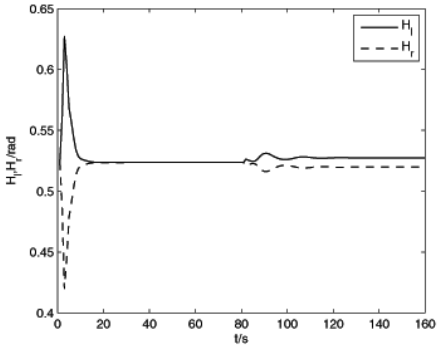


Figure 13. Asymmetric wing sweep angles.

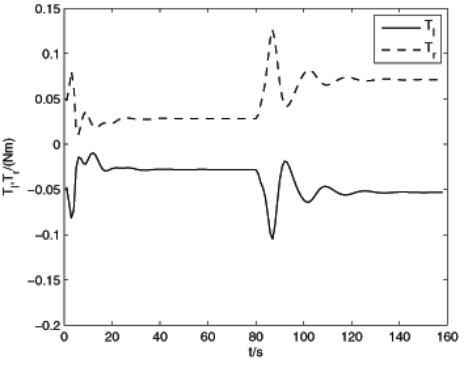


Figure 14. Wing sweep control torque.

We can see that the attack angle α increases as the UAV starts climbing, while the side slip angle β is always maintained in a very small zone around zero. The flight path angle μ and roll angle □ are negative in the helix flight stage because the UAV is doing a left turning. Figure 11 shows the angular rates of the UAV, which all converge to zero in the level flight. Fig. 12 gives the control surface deflections and the differential wing sweep angle. In the helix flight stage, δ_η is negative. This means that the left wing moves backward and the right wing moves forward as showed in Fig. 13, which then provide a negative rolling torque for the UAV. Fig. 14 gives the desired control torque for asymmetric wing sweep morphing. It can be seen that no actuator signal has reached the limits set by the command filter in this simulation, this means the desired trajectory is not too aggressive and the tracking errors can quickly converge to zero.

8.0 CONCLUSIONS

In this paper a multi-body dynamic model of an asymmetric sweep wing UAV is presented based on Kane's method. The UAV's transient behaviour during morphing and the morphing wing's dynamics are described in this model. A nonlinear trajectory tracking control system is presented then for the UAV based on the Kane's dynamic model. The control law is designed in an integrated way via constrained back-stepping method. Asymmetric wing sweep morphing is used as roll controller instead of aileron in the flight control, while the control of wing morphing itself is discussed as well.

https://doi.org/10.1017/S000192400000943X Published online by Cambridge University Press

Stability of the presented control law is discussed in the sense of Lyapunov. Numerical simulations of tracking a desired trajectory that contains two manoeuvres verifies the effectiveness of the designed control law and the feasibility of asymmetric wing morphing roll controller.

ACKNOWLEDGEMENTS

This work is supported by Natural Science Foundation of China under Grant 61273090.

REFERENCES

1. CLOUGH, B.T. Unmanned aerial vehicles: Autonomous control challenges, a researchers perspective, *J Aerospace Computing, Information and Communication*, 2005, **2**, (8), pp 327-347.
2. WEGENER, S., SULLIVAN, D., FRANK, J. and ENOMOTO, F. UAV Autonomous operations for airborne science missions, 2004, Third AIAA 'Unmanned Unlimited' Technical Conference,Workshop and Exhibition, AIAA Paper 2004-6416.
3. BAE, J.S. SEIGLER, T.M. and INMAN, D.J. Aerodynamic and static aeroelastic characteristics of a variable-span morphing wing, *J Aircr*, **42**, pp 528-534, 2005.
4. BOOTHE, K. A design scheme aimed at minimizing actuator and structural loads of a span morphing aircraft, 2006, 47th AIAA/ASME/ASCE/AHS/ASC Structures, Structural Dynamics and Materials Conference, pp 6418- 6427.
5. AN, J.G., YAN, M., ZHOU, W.B., SUN, X.H., YAN, Z. and QIU, C.R. Aircraft dynamic response to variable wing sweep geometry, *J Aircr*, March 1988, **25**, pp 216-221.
6. AN, J., MING, Y., WENBO, Z., XIANGHAI, S. and ZHEN, Y. The dynamic response of a variable sweep aircraft in the course of changing geometry, 1986, Atmospheric Flight Mechanics Conference, AIAA 1986-2234.
7. YUE, T., WANG, L. and AI, J. Multibody dynamic modeling and simulation of a tailless folding wing morphing aircraft, 2009, AIAA Atmospheric Flight Mechanics Conference, AIAA 2009-6155.
8. ABDULRAHIM, M. and LIND, R. Control and simulation of a multi-role morphing micro air vehicle, 2005, AIAA Paper 2005, 6481.
9. ABDULRAHIM, M. and LIND, R. Modeling and control of micro air vehicles with biologically-inspired morphing, 2006, American Control Conference, pp 2718-2723.
10. STANFORD, B., ABDULRAHIM, M., LIND, R. and IFJU, P. Design and optimization of morphing mechanisms for highly flexible micro air vehicles, 2006, 47th AIAA/ASME/ASCE/AHS/ASC Structures, Structural Dynamics and Materials Conference, AIAA 2006-2162.
11. ABDULRAHIM, M., GARCIA, H. and LIND, R. Flight characteristics of shaping the membrane wing of a micro air vehicle, *J Aircr*, 2005, **42**, pp 131-137.
12. HONG, C.H., CHEPLAK, M., CHOI, J.Y. and MAVRIS, D.N. Flexible multi-body design of a morphing UCAV, 2004, Third AIAA Unmanned Unlimited Technical Conference, pp 1-11.
13. SEIGLER, T.M. Dynamics and Control of Morphing Aircraft, 2005, PhD thesis, Virginia Polytechnic Institute and State University.
14. HURST, A.C., WICKENHEISER, A.M. and GARCIA, E. Control of an adaptive aircraft with a morphing input, 2009, 50th AIAA/ASME/ASCE/AHS/ASC Structures, Structural Dynamics and Materials Conference, AIAA- 2009-2130.
15. BOURDIN, P., GATTO, A. and FRISWELL, M.I. Performing co-ordinated turns with articulated wing-tips as multi-axis control effectors, *Aeronaut J*, Jan 2010, **114**, pp 35-47.
16. HENRY, J.J. Roll Control for UAVs by use of a Variable Span Morphing Wing, 2005, PhD thesis, University of Maryland.
17. GRANT, D.T. and LIND, R. Effects of time-varying inertias on flight dynamics of an asymmetric variable-sweep morphing aircraft, 2007, AIAA Atmospheric Flight Mechanics Conference, AIAA- 2007-6487.
18. TONG, L. and JI, H. Multibody dynamic modelling and roll control of asymmetric variable sweep morphing aircrafts, 2013, 10th IEEE International Conference on Control and Automation.
19. KANE, T.R. and LEVINSON, D.A. *Dynamics Theory and Applications*, 1985, McGraw-Hill Book Company.
20. TOWNSEND, M. Equivalence of Kane's, Gibbs-Appell's and Lagrange's equations, *J Guidance, Control, and Dynamics*, 1992, **15**, pp 1289-1292.

https://doi.org/10.1017/S000192400000943X Published online by Cambridge University Press

21. DESLOGE, E.A. Relationship between Kane's equations and the Gibbs-Appell equations, *J Guidance Control Dynamics*, 1987, **10**, pp 120-122.
22. KEAT, J. Comment on 'Relationship between Kane's equations and the Gibbs-Appell equations, *J Guidance, Control and Dynamics*, 1987, **10**, pp 594-595.
23. LEWIS, B.L. and STEVENS, F.L. *Aircraft Control and Simulation*, 1992, pp 1-54, 110-115, Wiley, New York, USA.
24. KAMINER, I., PASCOAL, A., HALLBERG, E. and SILVESTRE, C. Trajectory tracking for autonomous vehicles: An integrated approach to guidance and control, *J Guidance, Control and Dynamics*, 1998, **21**, pp 29-38.
25. SONNEVELDT, L., VAN OORT, E., CHU, Q. and MULDER, J. Nonlinear adaptive trajectory control applied to an F-16 model, J *Guidance, Control, and Dynamics,* , 2009, **32**, pp 25-39.
26. FARRELL, J., SHARMA, M. and POLYCARPOU, M. Backstepping-based flight control with adaptive function approximation, *J Guidance, Control and Dynamics*, 2005, **28**, pp 1089-1102.
27. ZHOU, H.B., PEI, H.L., HE, Y.-B. and ZHAO, Y.J. Trajectory tracking control of unmanned helicopter via filtering backstepping, *Control and Decision*, 2012, **27**, pp 613-617.
28. FARRELL, J., POLYCARPOU, M. and SHARMA, M. Adaptive backstepping with magnitude, rate and bandwidth constraints: aircraft longitude control, 2003, American Control Conference, pp 3898-3904.

https://doi.org/10.1017/S000192400000943X Published online by Cambridge University Press